



HAL
open science

Nanoparticle-Templated Self-Assembly of Viral Capsids Probed by Time-Resolved Absorbance Spectroscopy and X-Ray Scattering

Andrew Burke, Maelenn Chevreuil, Alisier Paris, Vanessa Delagrance, Claire Goldmann, Doru Constantin, Guillaume Tresset, Javier Pérez

► **To cite this version:**

Andrew Burke, Maelenn Chevreuil, Alisier Paris, Vanessa Delagrance, Claire Goldmann, et al.. Nanoparticle-Templated Self-Assembly of Viral Capsids Probed by Time-Resolved Absorbance Spectroscopy and X-Ray Scattering. *Physical Review Applied*, 2018, 10 (5), 10.1103/PhysRevApplied.10.054065 . hal-02348488

HAL Id: hal-02348488

<https://hal.science/hal-02348488>

Submitted on 5 Nov 2019

HAL is a multi-disciplinary open access archive for the deposit and dissemination of scientific research documents, whether they are published or not. The documents may come from teaching and research institutions in France or abroad, or from public or private research centers.

L'archive ouverte pluridisciplinaire **HAL**, est destinée au dépôt et à la diffusion de documents scientifiques de niveau recherche, publiés ou non, émanant des établissements d'enseignement et de recherche français ou étrangers, des laboratoires publics ou privés.

Nanoparticle-Templated Self-Assembly Dynamics of Viral Capsids Probed by UV-Vis Absorbance Spectroscopy and X-Ray Scattering

Andrew Burke, Maelenn Chevreuil, Alisier Paris, Vanessa Delagrangue,
Claire Goldmann, Doru Constantin,* and Guillaume Tresset†
*Laboratoire de Physique des Solides, CNRS, Univ. Paris-Sud,
Université Paris-Saclay, 91405 Orsay Cedex, France*

Javier Pérez
SOLEIL synchrotron, 91192 Gif-sur-Yvette Cedex, France
(Dated: October 4, 2018)

Viral capsid proteins have the remarkable ability to self-assemble around a cargo core, whether their genome, a polyelectrolyte or an inorganic nanoparticle. Although the equilibrium properties of such composite objects have been broadly investigated, little is known about the kinetic pathways leading to their assembly. By exploiting the plasmon resonance effect of gold nanoparticles, we show that the adsorption of viral proteins can be monitored through the redshift of the resonance wavelength. Kinetic measurements reveal that the process occurs in less than a second. The spatial arrangement of nanoparticles is probed by time-resolved small-angle X-ray scattering, and we observe the formation of transient aggregates with a lifetime in the hour range. The biocompatibility of gold nanoparticles induced by adsorbed proteins is of great importance for their use in biomedicine and the reported results should help better understand the processes of formation.

I. INTRODUCTION

The emerging study of biomolecular assemblies is an area of great fascination due to the astounding precision with which nanometer-sized objects are able to spontaneously assemble without any external intervention [1]. The assembly of viral proteins to form a capsid – i.e., the protein shell of a virus – is one such process [2–8]. Understanding the underlying mechanisms is fundamental in transferring the principles onto synthetic and macroscopic materials. A recent point of intrigue concerns how the self-assembly of viral proteins occurs around another material, e.g., the viral genome [9–18], a synthetic polymer [19–24] or a nanoparticle [25–33].

Gold nanoparticles (AuNPs) are of particular interest because they hold a lot of potential applications in photonics, electronics and biomedicine [34]. Once materials are reduced to nanometer sizes, a variety of interesting properties emerge, which are not seen in bulk materials. These distinctive optical and electromagnetic properties can be modified by changing parameters such as the size, shape and surface charge density of the nanoparticle in order to tune them for a particular function [35]. The existence of the surface plasmon resonance at the interface between a noble metal nanoparticle and the surrounding medium, serves to enhance the electromagnetic properties, notably absorption and scattering, in a way which is characteristic to each type of metal nanoparticle [36]. For biomedical applications in particular, it is crucial that nanoparticles are well stabilized because aggregation prevents them from diffusing through the tis-

sues and shortens their circulatory lifetime. Within this framework, the capsid formed by viral proteins around a synthetic core constitutes an efficient and biocompatible stabilizing agent as well as a protective barrier for the body.

The simplest viruses are made up of a capsid protecting the genome in the form of nucleic acids. Half of the viruses on Earth display an icosahedral symmetry and the capsid proteins are therefore arrayed onto an icosahedral lattice forming a two-dimensional crystal structure [37–39]. For example, brome mosaic virus (BMV) and cowpea chlorotic mottle virus (CCMV) are both single-stranded RNA viruses infecting plants, and their icosahedral capsid comprises 90 dimeric subunits that can self-assemble *in vitro* depending upon ionic conditions. The proteins interact with each other through a short-range hydrophobic and/or van der Waals attraction and a long-range electrostatic repulsion [40–42], while the subunit-genome, or subunit-cargo, interaction is realized by an electrostatic attraction. Daniel and coworkers [43] showed that the higher the surface charge density of ligand-stabilized AuNPs, the better their encapsulation into capsids derived from BMV. Theoretical investigations demonstrated that a threshold surface charge density must be exceeded and that the encapsulation efficiency is gradual due to charge regulation and size polydispersity of the nanoparticles [31]. He and coworkers [29] observed that the capsid of hepatitis B virus can withstand an increase of the nanoparticle diameter or adapt to it by generating packing defects.

While the equilibrium properties of empty or filled viral capsids have been thoroughly studied, the associated kinetic pathways, in contrast, are still poorly understood. Time-course static light scattering [44, 45], resistive-pulse sensing through nanofluidic channel [46], atomic force microscopy [47, 48], nuclear magnetic reso-

* doru.constantin@u-psud.fr

† guillaume.tresset@u-psud.fr

nance [49], charge detection mass spectrometry [50] and¹³⁷ time-resolved small-angle X-ray scattering (TR-SAXS)¹³⁸ [51–55] have been used to shed some light on the self-¹³⁹ assembly dynamics of empty or nucleic acids-filled cap-¹⁴⁰ sids. The dynamics of AuNPs encapsulation is chal-¹⁴¹ lenging to probe, because the adsorption of capsid pro-¹⁴² teins occurs very rapidly and, consequently, techniques¹⁴³ with long acquisition times are ineffective. Malyutin and¹⁴⁴ Dragnea [30] carried out a kinetic study by time-course¹⁴⁵ light scattering and cryo-electron tomography on the en-¹⁴⁶ capsulation of AuNPs into BMV capsids. They reported¹⁴⁷ a two-step mechanism where aggregates of nanoparticles¹⁴⁸ are transiently formed upon the presence of proteins,¹⁴⁹ then stable capsids enclosing nanoparticles bud off the¹⁵⁰ aggregates.

In this work, we exploit the plasmon resonance effect¹⁴⁸ of AuNPs to probe the adsorption of CCMV capsid pro-¹⁴⁹ teins on ligand-stabilized AuNPs. We also study the ag-¹⁵⁰ gregation mechanism proposed by Malyutin and Dragnea¹⁵¹ with TR-SAXS and we clearly detect the formation of ag-¹⁵² gregates, which are subsequently dissociated over a long¹⁵³ timescale. We expect this study to promote further inves-¹⁵⁴ tigation on the self-assembly dynamics of nanoparticle-¹⁵⁵ templated viral capsids and to help design systems useful¹⁵⁶ to biomedical and imaging applications.

II. EXPERIMENTAL METHODS

A. CCMV virion purification

Cowpea chlorotic mottle virus (CCMV) is purified¹⁶⁴ from infected blackeye cowpea leaves (*Vigna unguiculata*)¹⁶⁵ following a protocol developed by Ali and Roossinck [56].¹⁶⁶ 140 g of infected leaves are homogenized with 300 mL of¹⁶⁷ 0.15 M sodium acetate *pH* 4.8 in a blender, then 300¹⁶⁸ mL of ice-cold chloroform are added and the solution is¹⁶⁹ stirred for 10 min. After 10 min of centrifugation at¹⁷⁰ 10 000 $\times g$, the virions are precipitated by stirring the¹⁷¹ aqueous upper phase for 30 min in 20 mM NaCl and 8%¹⁷² of poly(ethylene glycol) (MW 8000). After another cen-¹⁷³ trifugation at 10 000 $\times g$ for 10 min, the pellet is dissolved¹⁷⁴ in 21 mL of 50 mM sodium acetate *pH* 4.8 and stirred¹⁷⁵ for 1 h. The solution is centrifuged at 8000 $\times g$ for 10,¹⁷⁶ min and the supernatant is centrifuged through a 20%¹⁷⁷ (w/v) sucrose cushion at 150 000 $\times g$ for 2 h. The virions,¹⁷⁸ are collected in the pellet and stored in 50 mM sodium¹⁷⁹ acetate *pH* 4.8 at -80 °C until use. Samples are deemed¹⁸⁰ pure when the extinction ratio verifies $A_{260}/A_{280} > 1.60$.¹⁸¹

B. Capsid protein purification

10 mg of purified virions are dissociated by a 24-¹⁸³ h dialysis against 0.5 M CaCl₂, 1 mM ethylenedi-¹⁸⁴ amine tetra-acetic acid (EDTA) *pH* 8.0, 1 mM phenyl-¹⁸⁵ methylsulfonyl fluoride, 1 mM dithiothreitol, 50 mM¹⁸⁶ tris(hydroxymethyl)aminomethane (Tris)-HCl *pH* 7.5.¹⁸⁷

After 18 h of centrifugation at 150 000 $\times g$, 1-mL¹⁸⁸ aliquots of the supernatant are extracted and conserved¹⁸⁹ if $A_{280}/A_{260} > 1.65$. The capsid proteins are kept in their¹⁹⁰ assembled form in 0.5 M NaCl, 1 mM EDTA *pH* 8.0, 50¹⁹¹ mM sodium acetate *pH* 4.8 at 4 °C until use within two¹⁹² weeks after purification. The protein concentration is es-¹⁹³ timated with an extinction coefficient $\epsilon_{\text{percent}} = 8.34$ at¹⁹⁴ 280 nm.

C. Gold nanoparticle synthesis

We use three batches of gold nanoparticles (AuNPs),¹⁹⁵ synthesized by different methods: Most UV-Vis ab-¹⁹⁶ sorbance experiments are done with AuNPs synthesized¹⁹⁷ in toluene using oleylamine as a capping agent [57]. We¹⁹⁸ study the effect of ligand charge (see Figure 3) on par-¹⁹⁹ ticles obtained by a seed-growth method in aqueous so-²⁰⁰ lution [58]. Particles used in TR-SAXS experiments (see²⁰¹ Figure 5) are synthesized via an improved citrate method²⁰² [59]. Particle sizes are similar in all batches.

Two types of ligands, similar to those used by Daniel²⁰³ *et al.* [43], are used to functionalize the AuNPs:²⁰⁴ a nonionic thiolated surfactant, (1-mercaptoundec-11-²⁰⁵ yl)hexa(ethylene glycol), HS-C₁₁-EG₆-OH, denoted as²⁰⁶ MUDOL and its acidic (carboxylated) counterpart, HS-²⁰⁷ C₁₁-EG₆-CH₂COOH, denoted as EG₆-COOH. The lat-²⁰⁸ ter is purchased from ProChimia Surfaces (Poland). The²⁰⁹ AuNPs synthesized in water, initially stabilized by 0.5²¹⁰ mM CTAB, are incubated overnight with an excess of²¹¹ either ligand. Those synthesized in toluene are resus-²¹² pended in THF, functionalized and then transferred to²¹³ water. They are afterwards washed in pure water and²¹⁴ stored at room temperature.

D. Encapsulation of AuNPs into viral capsids

CCMV capsid proteins in the form of dimeric subunits²¹⁵ are initially dispersed in 0.5 M NaCl, 1 mM EDTA *pH*²¹⁶ 8.0 and 50 mM Tris-HCl *pH* 7.5, while AuNPs are in²¹⁷ pure water. For transmission electron microscopy and²¹⁸ static extinction spectroscopy, subunits and AuNPs are²¹⁹ dialyzed together against 50 mM NaCl, 1 mM EDTA *pH*²²⁰ 8.0 and 50 mM sodium acetate *pH* 4.8. Aniagyei *et al.*²²¹ [27] found that acidic *pH* renders the adsorbed CCMV²²² protein layer more compact at the surface of AuNPs than²²³ at neutral *pH*. However, EG₆-COOH-stabilized AuNPs²²⁴ are not fully stable at low *pH*. As a consequence, our at-²²⁵ tempts to carry out kinetics by mixing rapidly subunits²²⁶ and AuNPs in acidic buffer failed because the AuNPs²²⁷ precipitated before being stabilized further by the sub-²²⁸ units. Therefore, adsorption kinetics and TR-SAXS ex-²²⁹ periments are performed by mixing subunits, AuNPs and²³⁰ pure water in such a way that the final ionic strength is²³¹ about 0.1 M and the *pH* remains at 7.5. In all exper-²³² iments, the final protein concentration is within 0.1-0.3

188 g.L^{-1} and the subunit-to-AuNP molar ratio ranges from 231
 189 180:1 to 3600:1 so that proteins are in large excess.

III. RESULTS

A. Morphology of protein-coated AuNPs observed by electron microscopy

E. Transmission electron microscopy

191 $5 \mu\text{L}$ of sample solution is placed during 10 min on a
 192 carbon grid treated by glow discharge, and blotted with
 193 the edge of a filter paper. A drop of 1% (v/v) ammo-
 194 nium molybdate is deposited on the grid for 30 s, then
 195 removed with filter paper, and the grid is allowed to air
 196 dry for at least 10 min. Transmission electron microscopy
 197 (TEM) is performed with a JEOL JEM-2010 microscope
 198 equipped with a 200-kV field emission gun. The sam-
 199 ples are imaged with magnifications comprised between
 200 $\times 20\,000$ and $\times 50\,000$ and the images are collected with a
 201 Gatan Ultrascan 4K CCD camera at a defocus comprised
 202 between 1.5 and 3 μm .

F. UV-Vis absorbance spectroscopy

204 For static experiments, we measure the absorbance
 205 spectrum of dilute particles for wavelengths comprised
 206 between 400 and 1400 nm with an Agilent Cary 5000
 207 spectrometer. Samples are placed in polystyrene cuvettes
 208 with a 10-mm optical path.

209 For adsorption kinetics, we use a Biologic SFM-3000
 210 stopped-flow apparatus (France) equipped with a manual
 211 monochromator and a high sensitivity photomultiplier.
 212 The wavelength is set to 530 nm and the extinction is
 213 collected with a fixed time interval of 10 ms.

G. Time-resolved small-angle X-ray scattering

215 X-ray scattering measurements are performed with the 240
 216 SWING beamline at the SOLEIL synchrotron facility 241
 217 (Gif-sur-Yvette, France). The wavelength is set to $\lambda = 1.242$
 218 \AA and the sample-to-detector distance is 4 m, which pro- 243
 219 vides scattering wavenumbers q ($q = 4\pi/\lambda \sin(\theta/2)$ where 244
 220 θ is the scattering angle) ranging from 2.3×10^{-3} to 0.28 245
 221 \AA^{-1} . Two-dimensional scattering images are recorded 246
 222 on an AVIEX large area CCD detector with an exposure 247
 223 time of 250 ms. The rapid mixing of AuNPs with sub- 248
 224 units is carried out with a Biologic SFM-300 stopped-flow 249
 225 apparatus (France) equipped with three syringes and the 250
 226 flow is stabilized by a hard stop valve. The scattering 251
 227 intensities are converted into absolute units after sub- 252
 228 tracting the contribution of the buffer, and the uncer- 253
 229 tainties are calculated after circular averaging using the 254
 230 FOXTROT software package. 255

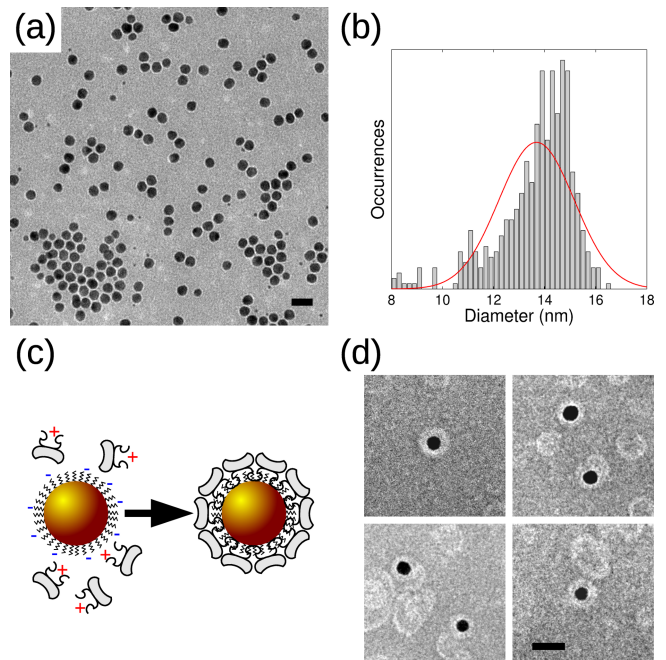


FIG. 1. Transmission electron microscopy of naked and protein-coated $\text{EG}_6\text{-COOH}$ -stabilized AuNPs. (a) Naked AuNPs and (b) their size distribution inferred from TEM images. (c) Schematics depicting the coating of ligand-stabilized AuNPs by subunits. (d) Protein-coated AuNPs. Scale bars are 30 nm.

234 Figure 1(a) shows a TEM image of naked $\text{EG}_6\text{-COOH}$ -
 235 stabilized AuNPs in pure water after synthesis. Note
 236 that all AuNPs used in this study are ligand-stabilized
 237 and naked AuNPs refers hereafter to as ligand-stabilized
 238 AuNPs without adsorbed proteins. Image analysis gives
 239 a diameter distribution of 13.7 ± 1.5 (mean \pm s.d.) nm
 [Fig. 1(b)], that is, the AuNPs are fairly monodisperse.
 At neutral $p\text{H}$ and high ionic strength (0.5 M), CCMV
 capsid proteins are in the form of dimeric subunits. Each
 subunit carries two flexible, cationic arms rich in argi-
 nine. When $\text{EG}_6\text{-COOH}$ -stabilized AuNPs and subunits
 are mixed at neutral $p\text{H}$ and low ionic strength (~ 0.1
 M), the cationic arms are electrostatically attracted by
 the anionic moiety of the ligands. As a result, the sub-
 units are adsorbed at the surface of the nanoparticles and
 form a capsid with some defects [Fig. 1(c)]; when the $p\text{H}$
 becomes acidic, the capsids are consolidated. Figure 1(d)
 depicts such AuNPs encapsulated into viral capsids. The
 size of the capsids is close to that of the native virions,
 i.e., 28 nm, and since the subunits are in excess, several
 empty capsids or pieces of capsids are coexisting with the
 protein-coated AuNPs.

B. Redshift of plasmon resonance induced by capsid proteins

A homogeneous nano-sized gold sphere embedded in a uniform electric field has a polarizability α (defined as the ratio between the induced dipole moment of the sphere and the applied electric field) given by [60]:

$$\alpha = 3V \frac{(\epsilon_S - \epsilon_W)(\epsilon_{Au} + 2\epsilon_S) + f(2\epsilon_S + \epsilon_W)(\epsilon_{Au} - \epsilon_S)}{(\epsilon_{Au} + 2\epsilon_S)(\epsilon_S + 2\epsilon_W) + 2f(\epsilon_S - \epsilon_W)(\epsilon_{Au} - \epsilon_S)} \quad (1)$$

where $f = [R/(R+d)]^3$ with R the radius of the AuNP and d the shell thickness. ϵ_S denotes the relative permittivity of the shell layer.

Changes in α can be probed using UV-Vis absorbance spectroscopy, since the beam extinction E is proportional to the extinction cross-section: $E = N\sigma_{\text{ext}}l/\ln(10)$, where N is the number of nanoparticles per unit volume and l is the length of optical path. The extinction cross-section σ_{ext} is the sum of the contributions arising from absorption and scattering. The scattering contribution is here negligible due to the small size of the nanoparticles. Therefore, σ_{ext} is dominated by the absorption cross section σ_{abs} :

$$\sigma_{\text{ext}} \approx \sigma_{\text{abs}} = \frac{2\pi}{\lambda_W} \Im(\alpha) \quad (2)$$

with λ_W the wavelength of the incident light in water and $\Im(\alpha)$ the imaginary part of α . Despite its simplicity, the model is quite accurate and allows extracting reliable parameters via full-curve fitting of the extinction curves [61].

Figure 2(a) gives the calculated absorption cross sections [Eq. (2)] of AuNPs coated with a dielectric shell. Note that the refractive index n is related to the relative permittivity ϵ by $\epsilon = n^2$. ϵ_{Au} is a complex function of the wavelength and is derived from an analytical model (see Appendix). In the absence of a shell, i.e., when $n_S = n_W$, the absorption cross-section exhibits a plasmon resonance peak at a wavelength around 520 nm. As the refractive index of the shell increases, the peak shifts to higher values and the maximal amplitude increases. The shift of wavelength between the spectrum with no shell and that with $n_S = 1.4$ is 3 nm, and amounts to 8 nm when $n_S = 1.5$. The ratio of the maximal amplitudes is found to be 1.10 and 1.23, respectively. The refractive index of proteins is known to lie in the range of 1.45 and 1.65 [62], and the thickness of a CCMV capsid is 5 nm [63]. We expect thus to have similar effects on experimental measurements.

Figure 2(b) shows the experimental extinction spec-

$$\alpha = 3V \frac{\epsilon_{Au} - \epsilon_W}{\epsilon_{Au} + 2\epsilon_W}$$

tra measured on naked and protein-coated AuNPs. The spectrum of naked AuNPs is fitted with a model of gold spheres having a radius of 7 nm. The spectrum of

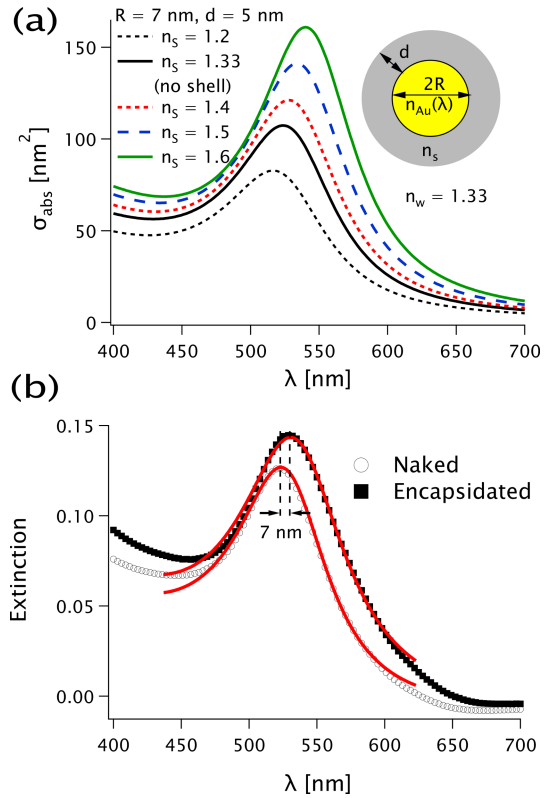


FIG. 2. UV-Vis absorbance spectroscopy of protein-coated AuNPs. (a) Calculated absorption cross-section of spherical AuNPs with a radius $R = 7$ nm and coated with a dielectric shell of thickness $d = 5$ nm with varying refractive indices n_S . (b) Experimental extinction spectra of naked and protein-coated AuNPs stabilized with EG₆-COOH ligands. The red solid lines are theoretical models fitting the measurements by using $R = 7$ nm, and either no shell (for the naked AuNPs, \circ) or a shell with $d = 5$ nm and $n_S = 1.44$ (for the encapsulated spheres, \blacksquare).

tra measured on naked and protein-coated AuNPs. The spectrum of naked AuNPs is fitted with a model of gold spheres having a radius of 7 nm. The spectrum of

307 protein-coated AuNPs is fitted with the same model of 337
 308 gold spheres, but coated with a 5-nm-thick protein layer,³³⁸
 309 yielding a refractive index $n_S = \sqrt{\epsilon_S} = 1.44$. The shift of³³⁹
 310 the resonance wavelength is found to be 7 nm. The fit³⁴⁰
 311 ting values are in agreement with the expected thickness³⁴¹
 312 and relative permittivity of a protein capsid. ³⁴²

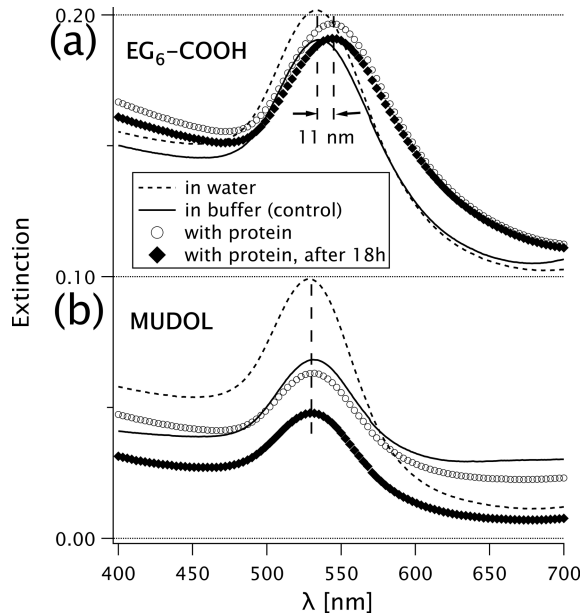


FIG. 3. Effect of ligands on the coating of AuNPs by proteins. Extinction spectra of AuNPs stabilized by (a) EG₆-COOH and (b) MUDOL ligands in pure water (dashed line), in buffer solution (solid line), in buffer solution just after mixing with capsid proteins (open discs), and in buffer solution 18 h after mixing with capsid proteins (full diamonds).

313 Figures 3(a) and (b) show the effect of ligands on the
 314 coating of AuNPs by viral proteins. The extinction spec-
 315 tra of AuNPs in pure water and in buffer solution are
 316 similar for both ligands, there is therefore no immediate
 317 effect of the buffer solution on AuNPs. More importantly,
 318 the extinction of EG₆-COOH-stabilized AuNPs in the
 319 presence of proteins exhibits a redshift of the resonance³⁴⁵
 320 wavelength of 9 nm, whereas the resonance remains at³⁴⁶
 321 the same wavelength for MUDOL-stabilized AuNPs with³⁴⁷
 322 proteins. This difference demonstrates that proteins are³⁴⁸
 323 adsorbed on EG₆-COOH-stabilized AuNPs but not on³⁴⁹
 324 MUDOL-stabilized AuNPs: The surface charge density³⁵⁰
 325 of AuNPs has to be negative and sufficiently high in ab-³⁵¹
 326 solute value to allow the adsorption of proteins, in good³⁵²
 327 agreement with the findings reported by Daniel *et al.*³⁵³
 328 [43]. The fact that the shift is 9 nm while it is 7 nm in³⁵⁴
 329 the previous measurements [Fig. 2(b)] may arise from a³⁵⁵
 330 slightly larger average thickness of the protein shell due³⁵⁶
 331 to experimental variations in the subunit-to-AuNP molar³⁵⁷
 332 ratios. The extinction of MUDOL-stabilized AuNPs in³⁵⁸
 333 the presence of proteins after 18 h is significantly lower³⁵⁹
 334 than immediately after mixing [Fig. 3(b)], unlike the³⁶⁰
 335 case of EG₆-COOH-stabilized AuNPs in the presence of³⁶¹
 336 proteins [Fig. 3(a)]. Because MUDOL-stabilized AuNPs³⁶²

have a neutral surface charge density and are not further
 stabilized by a layer of proteins, they massively aggregate
 due to strong attractive van der Waals forces and precipi-
 tate at the bottom of the tube. As a consequence, the
 concentration of AuNPs in the supernatant drops and so
 does the extinction.

C. Adsorption dynamics of proteins on nanoparticles

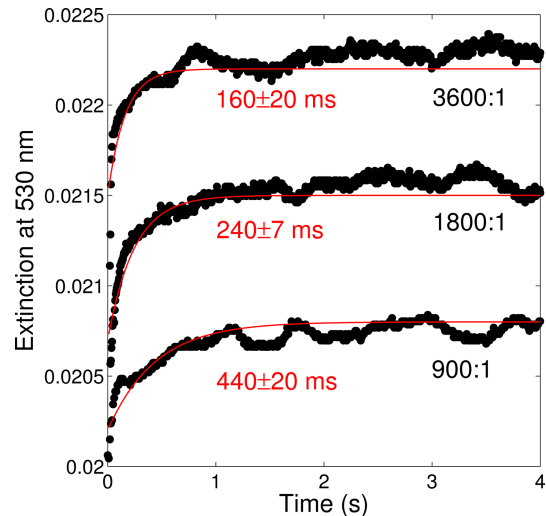


FIG. 4. Time-resolved extinction of protein-coated AuNPs, at various subunit-to-AuNP molar ratios. The red lines are exponential decay fits and the numbers in red are the corresponding decay times. The curves are shifted for clarity.

We investigate now the adsorption dynamics of proteins on EG₆-COOH-stabilized AuNPs in neutral buffer. Proteins and AuNPs are rapidly mixed and the extinction at 530 nm is monitored during the course of protein adsorption. As proteins are adsorbed on AuNPs, the wavelength of the plasmon resonance is gradually shifted from 520 nm to 530 nm in such a way that the extinction measured at 530 nm increases. Figure 4 gives the corresponding traces for three different molar ratios, with proteins in large excess. The adsorption occurs very rapidly, i.e., within a few hundreds of milliseconds. The adsorption timescale τ_{ads} decreases when the protein concentration c_S increases in such a way that $\tau_{\text{ads}} \propto c_S^{-0.8 \pm 0.2}$. A purely diffusion-limited process would yield $\tau_{\text{ads}} \propto c_S^{-1}$. The slight difference in the exponent may be due to a free energy barrier, most likely arising from the adsorbed subunits hindering the insertion of incoming free subunits through steric and electrostatic repulsions.

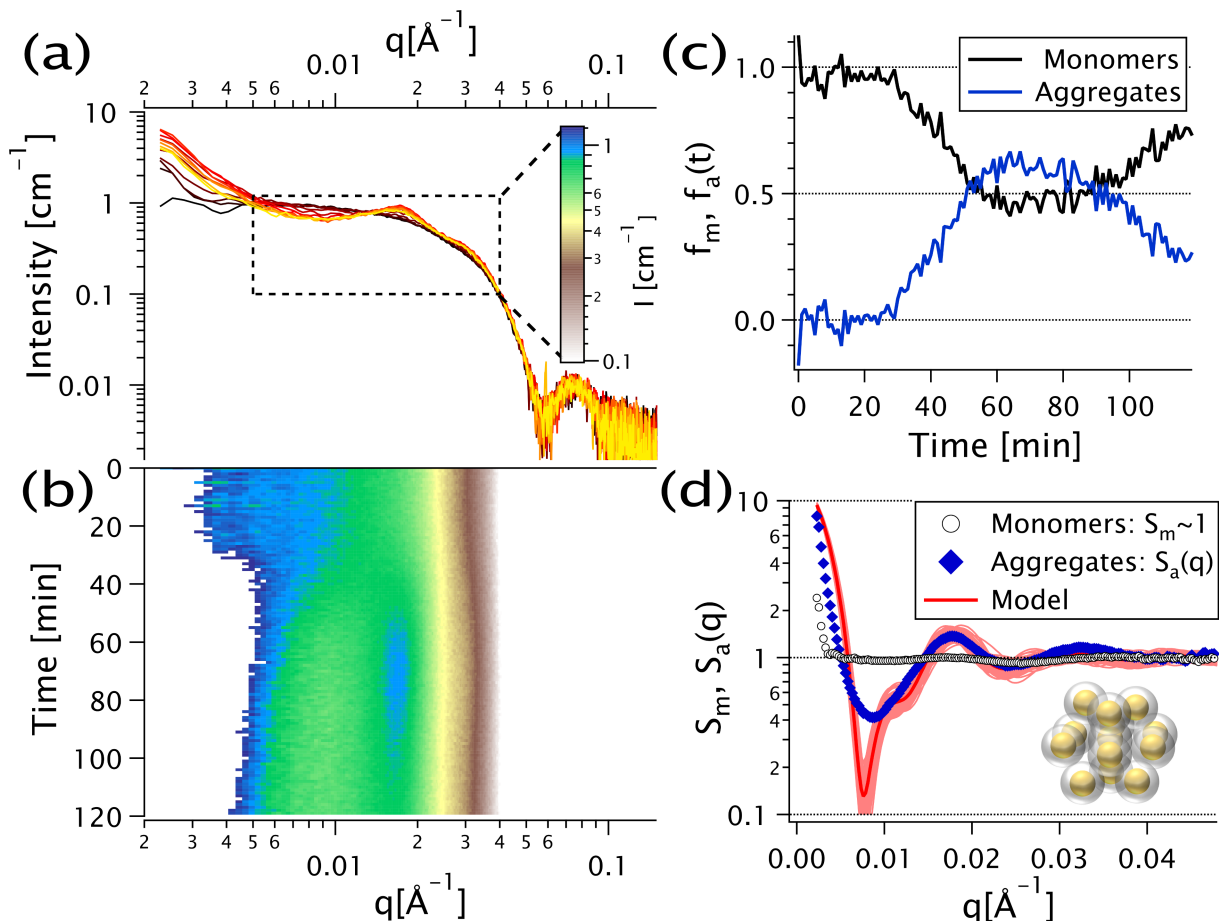


FIG. 5. Time-resolved small-angle X-ray scattering of EG₆-COOH-stabilized AuNPs coated by capsid proteins. (a) Scattering patterns collected at different time steps. (b) Two-dimensional representation of the scattering intensities as a function of time and wavenumber for the area delimited by the dashed box in (a). (c) Molar fractions of monomers (free protein-coated AuNPs) f_m and protein-coated AuNPs within aggregates f_a as a function of time inferred from singular value decomposition. (d) Corresponding structure factors of monomers $S_m(q)$ and aggregates $S_a(q)$. The light red lines are one hundred calculated structure factors of aggregates made of 13 particles separated by a distance fluctuating around 43 nm (3D model in inset) and the dark red line is their average. The protein concentration is 0.13 g.L⁻¹ and the subunit-to-AuNP molar ratio is 2640:1.

D. Assembly and dissociation dynamics of aggregates made of protein-coated AuNPs

Next, we probe the large-scale structures formed by protein-coated AuNPs by using TR-SAXS with a high-brilliance synchrotron source. Because the electron density of gold is considerably higher than that of proteins, the scattering intensity arising from capsid proteins is negligible with respect to that due to AuNPs. However, if the protein-coated AuNPs transiently form aggregates as reported by Malyutin and Dragnea [30], the presence of the latter can be readily detected via the modulation they induce in the structure factor.

Figure 5(a) shows the apparition of a peak at $q \simeq 0.018 \text{ \AA}^{-1}$, due to loosely-packed AuNPs aggregates. The two-dimensional representation of Fig. 5(b) reveals that the peak (visible as a blue streak) appears about 50 min after mixing subunits and AuNPs, and disappears almost completely after 110 min. The isosbestic points on the

scattering intensities of Fig. 5(a) at $q \simeq 5.5 \times 10^{-3}$ and 0.013 \AA^{-1} suggest the presence of only two species: free (monomers) and aggregated protein-coated AuNPs, interconverting over the course of the process, in which case the scattering intensity $I(q, t)$ reduces to [64]:

$$I(q, t) \propto [f_m(t) + f_a(t)S_a(q)]P(q) \quad (3)$$

where f_m and f_a stand for the molar fractions of free protein-coated AuNPs and protein-coated AuNPs within aggregates, respectively. $S_a(q)$ is the structure factor of the aggregates and $P(q)$ is the form factor of AuNPs. $S_a(q)$ must be seen as a structure factor averaged over all aggregates, during the whole process. $P(q)$ is obtained from the first scattering pattern, when protein-coated AuNPs are still all free in solution. The molar fractions and $S_a(q)$ are estimated by retaining the two first components of a singular value decomposition [65]

performed on $I(q)/P(q)$. By rotating and rescaling the basis vectors in order to reproduce the flat structure factor of monomers, i.e., $S_m(q) \sim 1$, $f_m(t)$ can be estimated. $f_a(t)$ and $S_a(q)$ are then deduced by mass conservation. $f_m(t)$ and $f_a(t)$ are plotted in Fig. 5(c). The first aggregates appear about 30 min after mixing and their fraction continues to grow until $t \simeq 60$ min. At this moment, around 60% of AuNPs are within aggregates. Then, AuNPs are slowly released but 2 h after mixing there are still $f_a = 25\%$ in aggregated form.

E. Modeling the structure factor of the aggregates

The structure factor of the aggregates $S_a(q)$ is shown in Fig. 5(d). Since all interactions are presumably isotropic, we describe it based on a compact reference assembly comprising 13 particles, one in the center and the remaining twelve forming a shell around it. The distance between nearest neighbors is initially 43 nm, but the particles are then allowed to fluctuate at random around their equilibrium positions according to Gaussian distributions with standard deviation 6.45 nm along each space dimension (x, y, z) . The structure factors corresponding to one hundred noise realizations are shown in light red and their average in dark red.

Despite its simplicity, the model is in qualitative agreement with the experimental data: the soft peak at 0.018 \AA^{-1} , indicative of a limited degree of order (as for an amorphous packing) is well captured. The discrepancies: a sharp minimum at 0.0076 \AA^{-1} and a rounded increase at lower q values, can be explained by the size polydispersity of the aggregates in solution. Note that the scattering signal is largely dominated by the gold nanoparticles and provides no direct information on the position and conformation of the proteins.

Given that the diameter of AuNPs is 15 nm as inferred from $P(q)$, EG₆-COOH ligand is 2 nm long at most, and the thickness of a CCMV capsid is 5 nm, the full diameter of protein-coated AuNPs is estimated to be 29 nm. In other words, the surfaces of protein-coated AuNPs within an aggregate are separated by a gap of 15 nm, most likely filled with capsid proteins. In another experiment where the subunit-to-AuNP molar ratio is reduced by a factor of two while keeping the subunit concentration identical, the structure peak is barely visible and there is almost no evolution of the scattering patterns. It suggests that the subunit-to-AuNP molar ratio as well as the subunit concentration have to be sufficiently high to induce the formation of transient aggregates.

IV. CONCLUSION

By combining UV-Vis absorbance spectroscopy and TR-SAXS, we probe the self-assembly of CCMV capsids templated by ligand-stabilized AuNPs with different temporal and spatial scales. The measurements allow

us to propose a three-step pathway: Right after mixing proteins and ligand-stabilized AuNPs, the proteins, driven by electrostatic interactions, adsorb on the AuNPs provided that the surface charge density is negative and high enough in absolute value. The adsorption occurs on the subsecond timescale and is accelerated when the subunit-to-AuNP molar ratio increases. In a large excess of subunits, a part of the protein-coated AuNPs form aggregates in coexistence with the remaining free protein-coated AuNPs within the first hour. The surface-to-surface distance between protein-coated AuNPs within an aggregate is sufficiently large to accommodate two or three layers of capsid proteins, and each aggregate comprises a dozen or so nanoparticles. Notice that the aggregates are soluble and do not precipitate at the bottom of the tube. Then, the aggregates slowly dissociate over a couple of hours by releasing individual protein-coated AuNPs. The latter are stable over long durations and electron microscopy images reveal a closed shell wrapping up each AuNP.

There is a need to better understand and subsequently, control the nonequilibrium self-assembly and self-organization dynamics of complex molecular systems [66]. Biological systems, spurred by the pressure of their own survival, have evolved to spontaneously build up large-scale, perfectly ordered structures in an error-free manner, despite an often adverse environment. The present work highlights the robustness and adaptability of viral proteins during the packaging of a cargo, as it efficiently occurs in host cell. It should promote further fundamental studies on bio-inspired systems, notably related to the physics of dynamical phenomena.

ACKNOWLEDGMENTS

M.C. is supported by the "IDI 2016" project funded by the IDEX Paris-Saclay, ANR-11-IDEX-0003-02. G.T. acknowledges financial support from the Agence Nationale de la Recherche (contract ANR-16-CE30-0017-01). We also acknowledge the SOLEIL synchrotron for allocation of synchrotron beam time on the SWING beamline. The electron microscopy imaging is supported by "Investissements d'Avenir" LabEx PALM (ANR-10-LABX-0039-PALM).

Appendix: Analytical model of the dielectric function of gold

The relative permittivity of gold is approximated by the analytical model used by Etchegoin *et al.* [67]:

$$\epsilon_{\text{Au}} = \epsilon_{\infty} - \frac{1}{\lambda_p^2 \left(\frac{1}{\lambda^2} + \frac{i}{\gamma_p \lambda} \right)} + \sum_{i=1,2} \frac{A_i}{\lambda_i} \left[\frac{e^{i\phi_i}}{\frac{1}{\lambda_i} - \frac{1}{\lambda} - \frac{1}{\gamma_i}} + \frac{e^{-i\phi_i}}{\frac{1}{\lambda_i} + \frac{1}{\lambda} + \frac{1}{\gamma_i}} \right].$$

494 The first two terms come from the Drude model while
 495 the summation is over two terms which come from inter-
 496 band transitions. λ_p is the plasma wavelength, γ_p is the

497 damping expressed as a wavelength, A_i is the amplitude
 498 of each term, λ_i and γ_i are the wavelength and damping
 499 of the respective interband transitions. ϕ_i is the phase of
 500 each transition. The parameter values correspond to the
 501 Johnson and Christy data [68], with the exception of λ_1 ,
 502 which we modify slightly to obtain better agreement with
 503 the spectrum of the naked particles: $\epsilon_{\infty} = 1.54$, $\lambda_p = 143$
 504 nm, $\gamma_p = 14500$ nm, $A_1 = 1.27$, $\phi_1 = -\pi/4$, $\lambda_1 = 445$
 nm (470 nm for Johnson and Christy), $\gamma_1 = 1900$ nm,
 $A_2 = 1.1$, $\phi_2 = -\pi/4$, $\lambda_2 = 325$ nm and $\gamma_2 = 1060$ nm.

-
- 507 [1] Q. Luo, C. Hou, Y. Bai, R. Wang, and J. Liu, *Chem.*
 508 *Rev.* **116**, 13571 (2016). 555
- 509 [2] W. H. Roos, R. Bruinsma, and G. J. L. Wuite, *Nat.*
 510 *Phys.* **6**, 733 (2010). 557
- 511 [3] M. G. Mateu, *Arch. Biochem. Biophys.* **531**, 65 (2013). 558
- 512 [4] G. Tresset, V. Decouche, J.-F. Bryche, A. Charpilienne,
 513 C. Le Coeur, C. Barbier, G. Squires, M. Zeghal, D. Pon-
 514 cet, and S. Bressanelli, *Arch. Biochem. Biophys.* **537**,
 515 144 (2013). 562
- 516 [5] M. F. Hagan, *Adv. Chem. Phys.* **155**, 1 (2014). 563
- 517 [6] R. F. Bruinsma and W. S. Klug, *Annu. Rev. Condens.*
 518 *Matter Phys.* **6**, 245 (2015). 565
- 519 [7] J. D. Perlmutter and M. F. Hagan, *Annu. Rev. Phys.*
 520 *Chem.* **66**, 217 (2015). 567
- 521 [8] T. Verdier, L. Foret, and M. Castelnovo, *J. Phys. Chem.*
 522 *B* **120**, 6411 (2016). 569
- 523 [9] R. Zandi and P. van der Schoot, *Biophys. J.* **96**, 9 (2009). 570
- 524 [10] M. Comas-Garcia, R. D. Cadena-Nava, A. L. N. Rao,
 525 C. M. Knobler, and W. M. Gelbart, *J. Virol.* **86**, 12271
 526 (2012). 573
- 527 [11] A. Borodavka, R. Tuma, and P. G. Stockley, *Proc. Natl.*
 528 *Acad. Sci. U. S. A.* **109**, 15769 (2012). 575
- 529 [12] M. Castelnovo, D. Muriaux, and C. Faivre-Moskalenko,
 530 *New J. Phys.* **15**, 035028 (2013). 577
- 531 [13] A. Zlotnick, J. Z. Porterfield, and J. C.-Y. Wang, *Bio-*
 532 *phys. J.* **104**, 1595 (2013). 579
- 533 [14] R. F. Garmann, M. Comas-Garcia, A. Gopal, C. M. Kno-
 534 bler, and W. M. Gelbart, *J. Mol. Biol.* **426**, 1050 (2014). 581
- 535 [15] N. Patel, E. C. Dykeman, R. H. A. Coutts, G. P.
 536 Lomonosoff, D. J. Rowlands, S. E. V. Phillips, N. Ran-
 537 son, R. Twarock, R. Tuma, and P. G. Stockley, *Proc.*
 538 *Natl. Acad. Sci. U. S. A.* **112**, 2227 (2015). 585
- 539 [16] R. F. Bruinsma, M. Comas-Garcia, R. F. Garmann, and
 540 A. Y. Grosberg, *Phys. Rev. E Stat. Nonlin. Soft Matters*
 541 *Phys.* **93**, 032405 (2016). 588
- 542 [17] R. F. Garmann, M. Comas-Garcia, C. M. Knobler, and
 543 W. M. Gelbart, *Acc. Chem. Res.* **49**, 48 (2016). 590
- 544 [18] S. Li, G. Erdemci-Tandogan, P. van der Schoot, and
 545 R. Zandi, *J. Phys. Condens. Matter* **30**, 044002 (2018). 592
- 546 [19] F. D. Sikkema, M. Comellas-Aragons, R. G. Fokkink,
 547 B. J. M. Verduin, J. J. L. M. Cornelissen, and R. J. M.
 548 Nolte, *Org. Biomol. Chem.* **5**, 54 (2007). 595
- 549 [20] Y. Hu, R. Zandi, A. Anavitarte, C. M. Knobler, and
 550 W. M. Gelbart, *Biophys. J.* **94**, 1428 (2008). 597
- 551 [21] O. M. Elrad and M. F. Hagan, *Phys. Biol.* **7**, 045003
 552 (2010). 599
- 553 [22] M. Comellas-Aragons, F. D. Sikkema, G. Delaittre, 600
 A. E. Terry, S. M. King, D. Visser, R. K. Heenan, R. J. M.
 Nolte, J. J. L. M. Cornelissen, and M. C. Feiters, *Soft*
Matter **7**, 11380 (2011).
- [23] R. D. Cadena-Nava, Y. Hu, R. F. Garmann, B. Ng, A. N.
 Zelikin, C. M. Knobler, and W. M. Gelbart, *J. Phys.*
Chem. B **115**, 2386 (2011).
- [24] G. Tresset, M. Tatou, C. Le Coeur, M. Zeghal,
 V. Bailleux, A. Lecchi, K. Brach, M. Klekotko, and
 L. Porcar, *Phys. Rev. Lett.* **113**, 128305 (2014).
- [25] J. Sun, C. DuFort, M.-C. Daniel, A. Murali, C. Chen,
 K. Gopinath, B. Stein, M. De, V. M. Rotello, A. Holzen-
 burg, C. C. Kao, and B. Dragnea, *Proc Natl Acad Sci*
U S A **104**, 1354 (2007).
- [26] N. L. Goicochea, M. De, V. M. Rotello, S. Mukhopad-
 hyay, and B. Dragnea, *Nano Lett.* **7**, 2281 (2007).
- [27] S. E. Anagyeyi, C. J. Kennedy, B. Stein, D. A. Willits,
 T. Douglas, M. J. Young, M. De, V. M. Rotello,
 D. Srisathiyarayanan, C. C. Kao, and B. Dragnea,
Nano Lett. **9**, 393 (2009).
- [28] C. C. DuFort and B. Dragnea, *Annu. Rev. Phys. Chem.*
61, 323 (2010).
- [29] L. He, Z. Porterfield, P. van der Schoot, A. Zlotnick, and
 B. Dragnea, *ACS Nano* **7**, 8447 (2013).
- [30] A. G. Mal'yutin and B. Dragnea, *J. Phys. Chem. B* **117**,
 10730 (2013).
- [31] R. Kusters, H.-K. Lin, R. Zandi, I. Tsvetkova, B. Drag-
 nea, and P. van der Schoot, *J. Phys. Chem. B* **119**, 1869
 (2015).
- [32] A. Liu, M. Verwegen, M. V. de Ruiter, S. J. Maassen,
 C. H.-H. Traulsen, and J. J. L. M. Cornelissen, *J. Phys.*
Chem. B **120**, 6352 (2016).
- [33] Z. Ye, L. Wei, X. Zeng, R. Weng, X. Shi, N. Wang,
 L. Chen, and L. Xiao, *Anal. Chem.* **90**, 1177 (2018).
- [34] E. C. Dreaden, A. M. Alkilany, X. Huang, C. J. Murphy,
 and M. A. El-Sayed, *Chem. Soc. Rev.* **41**, 2740 (2012).
- [35] M. Daniel and D. Astruc, *Chem. Rev.* **104**, 293 (2004).
- [36] V. Myroshnychenko, J. Rodriguez-Fernandez,
 I. Pastoriza-Santos, A. M. Funston, C. Novo, P. Mul-
 vaney, L. M. Liz-Marzan, and F. J. Garcia de Abajo,
Chem. Soc. Rev. **37**, 1792 (2008).
- [37] R. Zandi, D. Reguera, R. F. Bruinsma, W. M. Gelbart,
 and J. Rudnick, *Proc. Natl. Acad. Sci. U. S. A.* **101**,
 15556 (2004).
- [38] V. L. Lorman and S. B. Rochal, *Phys. Rev. Lett.* **98**,
 185502 (2007).
- [39] S. B. Rochal, O. V. Konevtsova, A. E. Myasnikova, and
 V. L. Lorman, *Nanoscale* **8**, 16976 (2016).

- [40] W. K. Kegel and P. van der Schoot, *Biophys. J.* **86**, 3905 (2004).
- [41] J. Chen, M. Chevreuil, S. Combet, Y. Lansac, and G. Tresset, *J. Phys. Condens. Matter* **29**, 474001 (2017).
- [42] G. Tresset, J. Chen, M. Chevreuil, N. Nhiri, E. Jacquet, and Y. Lansac, *Phys. Rev. Applied* **7**, 014005 (2017).
- [43] M.-C. Daniel, I. B. Tsvetkova, Z. T. Quinkert, A. Murali, M. De, V. M. Rotello, C. C. Kao, and B. Dragnea, *ACS Nano* **4**, 3853 (2010).
- [44] J. M. Johnson, J. Tang, Y. Nyame, D. Willits, M. J. Young, and A. Zlotnick, *Nano Lett.* **5**, 765 (2005).
- [45] C. Chen, C. C. Kao, and B. Dragnea, *J. Phys. Chem. A* **112**, 9405 (2008).
- [46] Z. D. Harms, L. Selzer, A. Zlotnick, and S. C. Jacobson, *ACS Nano* **9**, 9087 (2015).
- [47] M. Castellanos, R. Pérez, P. J. P. Carrillo, P. J. de Pablo, and M. G. Mateu, *Biophys. J.* **102**, 2615 (2012).
- [48] M. Medrano, M. A. Fuertes, A. Valbuena, P. J. P. Carrillo, A. Rodriguez-Huete, and M. G. Mateu, *J. Am. Chem. Soc.* **138**, 15385 (2016).
- [49] S. Milles, M. R. Jensen, G. Communie, D. Maurin, G. Schoehn, R. W. H. Ruigrok, and M. Blackledge, *Angew. Chem. Int. Ed.* **55**, 9356 (2016).
- [50] C. A. Lutomski, N. A. Lyktey, E. E. Pierson, Z. Zhao, A. Zlotnick, and M. F. Jarrold, *J. Am. Chem. Soc.* **140**, 5784 (2018).
- [51] S. Kler, R. Asor, C. Li, A. Ginsburg, D. Harries, A. Oppenheim, A. Zlotnick, and U. Raviv, *J. Am. Chem. Soc.* **134**, 8823 (2012).
- [52] G. Tresset, C. Le Coeur, J.-F. Bryche, M. Tatou, M. Zeghal, A. Charpilienne, D. Poncet, D. Constantin, and S. Bressanelli, *J. Am. Chem. Soc.* **135**, 15373 (2013).
- [53] D. Law-Hine, A. K. Sahoo, V. Bailleux, M. Zeghal, S. Prevost, P. K. Maiti, S. Bressanelli, D. Constantin, and G. Tresset, *J. Phys. Chem. Lett.* **6**, 3471 (2015).
- [54] D. Law-Hine, M. Zeghal, S. Bressanelli, D. Constantin, and G. Tresset, *Soft Matter* **12**, 6728 (2016).
- [55] M. Chevreuil, D. Law-Hine, J. Chen, S. Bressanelli, S. Combet, D. Constantin, J. Degrouard, J. Möller, M. Zeghal, and G. Tresset, *Nat. Commun.* **9**, 3071 (2018).
- [56] A. Ali and M. J. Roossinck, *J. Virol. Methods* **141**, 84 (2007).
- [57] H. Hiramatsu and F. E. Osterloh, *Chem. Mater.* **16**, 2509 (2004).
- [58] X. Ye, L. Jin, H. Caglayan, J. Chen, G. Xing, C. Zheng, V. Doan-Nguyen, Y. Kang, N. Engheta, C. R. Kagan, and C. B. Murray, *ACS Nano* **6**, 2804 (2012).
- [59] J. Piella, N. G. Bastús, and V. Puntès, *Chem. Mater.* **28**, 1066 (2016).
- [60] C. Bohren and D. R. Huffman, *Absorption and scattering of light by small particles* (Wiley-VCH, New York, 2008).
- [61] K. Slyusarenko, B. Abécassis, P. Davidson, and D. Constantin, *Nanoscale* **6**, 13527 (2014).
- [62] D. B. Hand, *J. Biol. Chem.* **108**, 703 (1935).
- [63] J. A. Speir, S. Munshi, G. Wang, T. S. Baker, and J. E. Johnson, *Structure* **3**, 63 (1995).
- [64] R. J. Hunter, *Foundations of colloid science* (Oxford University Press, New York, 2001).
- [65] E. R. Henry, *Biophys. J.* **72**, 652 (1997).
- [66] S. Whitelam and R. L. Jack, *Annu. Rev. Phys. Chem. Annual Review of Physical Chemistry*, **66**, 143 (2015).
- [67] P. G. Etchegoin, E. C. Le Ru, and M. Meyer, *J. Chem. Phys.* **125**, 164705 (2006).
- [68] P. Johnson and R. Christy, *Phys. Rev. B* **6**, 4370 (1972).